Palaeontology
The Palaeontological Association
www.palass.org

[Palaeontology, Vol. 57, Part 5, 2014, pp. 1059–1066]

FINITE ELEMENT, OCCLUSAL, MICROWEAR AND MICROSTRUCTURAL ANALYSES INDICATE THAT CONODONT MICROSTRUCTURE IS ADAPTED TO DENTAL FUNCTION

by CARLOS MARTÍNEZ-PÉREZ[1]*, EMILY J. RAYFIELD[1], MARK A. PURNELL[2] *and* PHILIP C. J. DONOGHUE[1]*

[1]School of Earth Sciences, University of Bristol, Wills Memorial Building, Queen's Road, Bristol, BS8 1RJ, UK; e-mails: carlos.martinez-perez@bristol.ac.uk, e.rayfield@bristol.ac.uk, phil.donoghue@bristol.ac.uk
[2]Department of Geology, University of Leicester, University Road, Leicester, LE1 7RH, UK; e-mail: map2@leicester.ac.uk
*Corresponding authors

Typescript received 8 November 2013; accepted in revised form 21 January 2014

Abstract: Conodonts constitute the earliest evidence of skeletal biomineralization in the vertebrate evolutionary lineage, manifest as a feeding apparatus of tooth-like elements comprised of enamel- and dentine-like tissues that evolved in parallel with these canonical tissues in other total-group gnathostomes. As such, this remarkable example of evolutionary parallelism affords a natural experiment in which to explore the constraints on vertebrate skeletal evolution. Using finite element analysis, informed by occlusal and microwear analyses, we tested the hypothesis that coincidence of complex dental function and microstructural differentiation in the enamel-like tissues of conodonts and other vertebrates is a consequence of functional adaptation. Our results show topological co-variation in the patterns of stress distribution and crystallite orientation. In regions of high stress, such as the apex of the basal cavity and inner parts of the platform, the crown tissue comprises interwoven prisms, discontinuities between which would have acted to decussate cracks, preventing propagation. These results inform a general occlusal model for platform conodont elements and demonstrate that the complex microstructure of conodont crown tissue is an adaptation to the dental functions that the elements performed.

Key words: conodont, function, occlusion, microwear, microstructure, finite element analysis.

CONODONTS are an extinct group of jawless vertebrates, the first in our evolutionary lineage to experiment with skeletal biomineralization. Manifest as an oropharyngeal feeding apparatus, the biomineralized skeletal elements are composed of two units: a basal body of dentine-like tissue (Sansom *et al.* 1994) and a crown of hypermineralized tissue comparable with the enamel of other skeletonizing vertebrates (Donoghue 1988). Despite their structural, topological and developmental similarities to these canonical vertebrate skeletal tissues (Donoghue 1998; Donoghue and Aldridge 2001), conodont skeletal tissues evolved independently and prior to those encountered in other skeletonizing vertebrates (Murdock *et al.* 2013). As such, this remarkable instance of convergence affords a natural experiment in which to explore the constraints on vertebrate skeletal evolution. Here, we present an integrative observational and computational experimental approach to testing the hypothesis that coincidence of complex dental function and microstructural differentiation in conodonts and other vertebrates is a consequence of functional adaptation (Donoghue 2001). Integral to this hypothesis is the apparently contentious interpretation of conodont elements as dental tools (Purnell 1994, 1995; Donoghue and Purnell 1999*a*, *b*; Jones *et al.* 2012*a*, *b*) and the observation that microstructural differentiation of conodont crown tissue coincides with, and is adapted to, implied dental stresses. This interpretation contrasts with the view of some contemporary authors (Blieck *et al.* 2010; Turner *et al.* 2010), that conodont elements were not used for food processing, merely acting as internal supports for an active suspension-feeding mechanism. This competing hypothesis has been roundly rejected on the observation that: (1) the conodont feeding apparatus does not show positive growth allometry, incompatible with the filter interpretation (Purnell 1994); (2) conodont elements exhibit surface microwear indicative of element–element dental function (Purnell 1995); (3) microwear loci coincide with

doi: 10.1111/pala.12102

element–element occlusal contact (Donoghue and Purnell 1999*a*); and (4) repair loci (indicative of episodic soft tissue cover of elements; Hass 1941) coincide with occlusal and microwear loci (Donoghue and Purnell 1999*b*).

To test the hypothesis that variations in the enamel-like crown tissue of conodonts is an adaptation to dental function, we undertook an integrative functional analysis of P_1 elements dissected from rare articulated remains of the Carboniferous ozarkodinid *Gnathodus bilineatus*. These tests encompass a finite element (FE) analysis constrained by characterization of occlusion and microwear, in parallel with a description of the microstructure. Our results inform a general occlusal model for platform conodont elements and demonstrate that the complex microstructure of conodont crown tissue is an adaptation to the dental functions that the elements performed.

MATERIAL AND METHODS

Our study is focused on isolated P_1 elements and bedding plane assemblages of *G. bilineatus* (Fig. 1), a close relative of *Idiognathodus*, the subject of previous qualitative functional interpretation (Purnell 1995; Purnell and Donoghue 1997; Donoghue and Purnell, 1999*a*). Articulated remains recovered from the Mississippian Heath Formation (Montana, USA) were used in the microwear and occlusion study. Isolated elements from Stonehead Beck, North Yorkshire (UK), provided additional data for analysis of microwear patterns and histology. All the specimens are deposited in the Natural History Museum, London (UK).

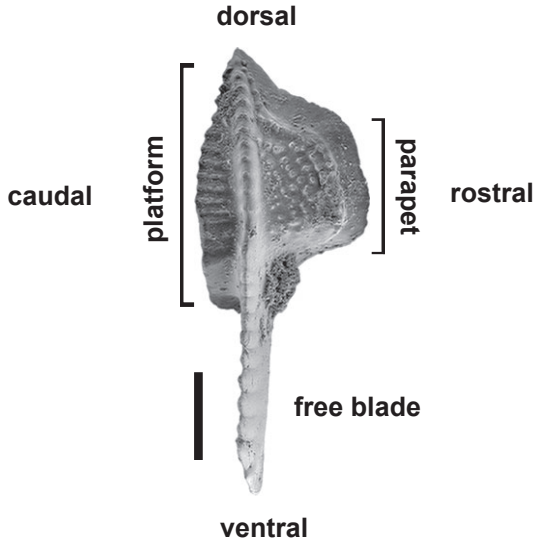

FIG. 1. Complete sinistral P_1 element of *Gnathodus bilineatus* showing the orientation and different morphological terms. Scale bar represents 50 μm.

Occlusal model

The analysis of occlusion is based on a pair of P_1 elements of *Gnathodus* from a natural assemblage of the Heath formation (Mississippian, Montana, USA). Occlusion was studied directly by placing the P_1 elements in opposition and held together with polyvinyl butyral adhesive during the SEM study. Additionally, to evaluate correctly the occlusion cycle, the pair of elements were also scanned with synchrotron X-ray tomographic microscopy (SRXTM), a noninvasive technique that allowed us to obtain accurate 3D and 2D digital models (Donoghue *et al.* 2006). The elements were scanned using the TOMCAT beamline at the Swiss Light Source, Paul Scherrer Institute, Villigen, Switzerland, with a 20× objective, exposure time at 12 keV was 500 ms, and 1001 projections were acquired equiangularly over 180 degrees. Projections were postprocessed and rearranged into flat- and darkfield-corrected sinograms, and reconstruction was performed on a 16-node Linux PC farm using highly optimized filtered back-projection routines. Isotropic voxel dimensions are 0.36 μm. Slice data derived from the scans were segmented using the software package AVIZO® for computed tomography (further details can be found in Donoghue *et al.* 2006). Finally, renderings were manipulated using the software Geomagic Studio® ver. 12 (Geomagic, Rock Hill, SC, USA) to reconstruct digitally the occlusion process (Fig. 2A–F).

Microwear data acquisition

Because some of the elements studied here are from articulated natural assemblages, they cannot have undergone post-mortem transport and consequently surface damage. Thus, the wear on the surfaces of these elements must have been produced *in vivo*, providing important and unequivocal corroboration of surface wear observed on specimens from collections of disarticulated elements. The microwear data were acquired from SEM images, and digital images captured using high-resolution focus variation optical microscopy (Alicona infinite focus microscope – IFM) following the protocol developed by Purnell and Jones (2012). This technique automatically captures an image stack from which a fully in-focus image is generated. Therefore, and following Purnell and Jones (2012), all images were acquired using fixed, co-axial illumination at constant magnification of ×50. Data were acquired from both the occlusal and nonocclusal sides of the blades and when the elements were too large for one field of view, several images were captured and automontaged within the IFM software.

For both techniques, specimens were sputter-coated with gold prior to imaging. The SEM study was under-

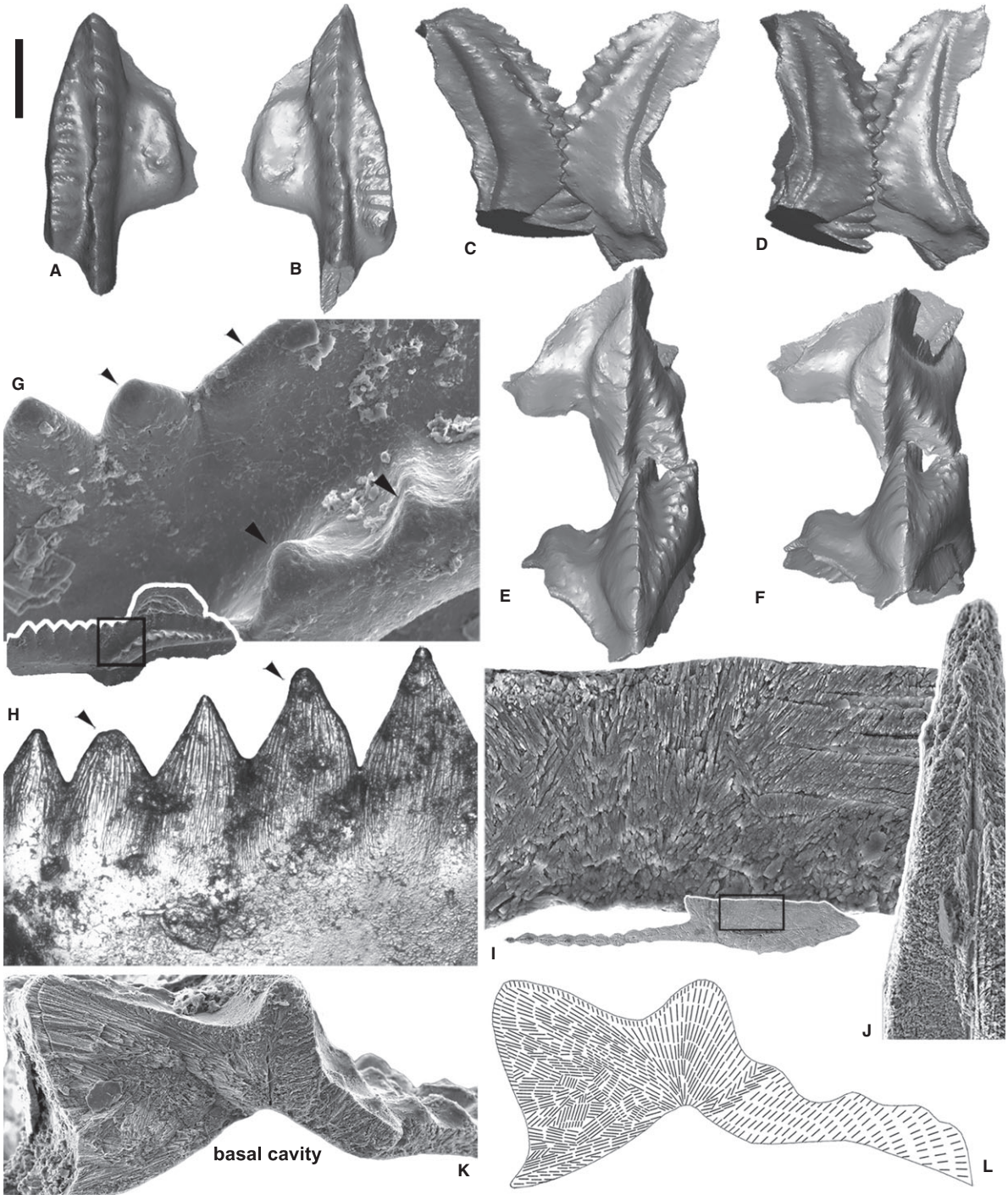

FIG. 2. *Gnathodus bilineatus* P_1 elements. A–F, tomographic models of the platforms from an occlusal pair dissected from an articulated skeleton; A–B, oral morphology of the sinistral and dextral elements (NHMUK PM X 3665 (1) and NHMUK PM X 3665 (2) respectively); C–F, occlusal cycle in caudal (C–D) and dorsal (E–F) views. G, *Gnathodus* platform showing smooth polishing of blade denticles and platform ridges (black arrows); inset indicates location on element (specimen lost during the photography process). H, spalls (black arrows) on the nonocclusal side of the blade (NHMUK PM X 3669). I, etched horizontal section showing the microstructural variation between the prismatic tissue of the ventral domain and the lamellar tissue of the dorsal domain; inset indicates location on section (NHMUK PM X 3666). J, transverse fracture of the blade showing the hydroxyapatite crystallites arranged subparallel to the external oral surfaces after etching (NHMUK PM X 3667). K, transverse artificial fracture of the ventral platform showing the microstructural variation after etching (NHMUK PM X 3668). L, diagrammatic summary of microstructure variation within the ventral domain. Scale bar represents: (A–F) 175 μm, (G) 25 μm, (H, J) 40 μm, (I, L) 30 μm, (K) 50 μm.

taken on a Hitachi S-3500N (University of Bristol) and on a Hitachi S-3600N (University of Leicester).

Histological samples preparation

For the histological study, more than 20 pristine-isolated P_1 elements of *G. bilineatus*, with CAI values of 1 (no thermal alteration), were used to elucidate the inner microstructure of the crown element. The elements were embedded in transparent polyester resin (Struers) prior to sectioning and were cut in transversal, sagittal or longitudinal section using a diamond blade on an Isomet low-speed saw (Buehler, Düsseldorf, Germany). These surfaces were ground until the desired plane of section was reached, using 800 and 1200 silicon carbide abrasive paper. Ground sections were then polished on a polishing pad with Kemet diamond polish paste and Kemet Type-W polishing lubricant (Kemet International, Maidstone, UK). Finally, the samples were etched using 0.5% orthophosphoric acid for 5–10 minutes prior to imaging in the SEM. The samples were repolished, etched and coated as many times as was necessary to elucidate the inner microstructure. We also studied the microstructure of artificial fractures produced using an entomological needle mounted in a pin vice by applying a force to the pit of the basal cavity, after the immersion of the specimens in a drop of water to prevent loss during the procedure. As with the resin-embedded elements, surfaces were etched using 0.5% orthophosphoric acid, always for less than 10 min, and coated later for SEM study.

FE models

To analyse the mechanical behaviour of the element platform under load conditions, an FE analysis, a conventional engineering technique used to analyse the stress and strain within complex shapes, was conducted. 3D models based on the SRXTM characterization of the *Gnathodus* natural assemblage pair and manipulated with the software Geomagic Studio® (Geomagic, USA) were used to reconstruct the occlusion process to identify the region of the platforms most constrained during the occlusal cycle (Fig. 3A–B). At this point, 2D transverse sections through right and left P_1 elements were created using *tpsDig* software to digitize cross-sectional outlines, which were imported into the COSMOSM FE software (SRAC, Los Angeles, CA, USA and CenitDesktop, Witney, UK) to analyse the mechanical behaviour of the platform by means of FE analysis. We undertook a two-dimensional FE analysis as: (1) our analysis revealed that the rotational occlusion of the elements resulted in element–element contact confined to small cross sections of their oral morphology at any one point in the occlusal cycle; and (2) we were able to identify this principal narrow area of functional element–element contact through our occlusal and microwear analyses. Our 2D plane is therefore an appropriate characterization of element morphology underlying this principal functional surface and should reflect the planar region of greatest load.

A right element model of 11 081 nodes and a left element model of 11 034 nodes were produced (Fig. 3C–D), comprising, respectively, 5781 and 5794 three-noded triangular FEs. Assuming a comparable histology for conodont crown tissue and vertebrate enamel, we applied homogeneous material properties to the model following the approximations of Jones *et al.* (2012*a*) for conodont hypermineralized tissue: Young's modulus = 60 GPa, Poisson ratio = 0.23 and density = 2.5 e^3 kg/m^3. The model was anchored at the basal cavity area with 179 nodes in the left element and 149 nodes in the right element, all fixed in 6 degrees of freedom. To simulate the occlusion loads, 1 N was distributed across the nodes of the oral surface, with the location of load determined according to the microwear patterns and the occlusion data previously obtained. The loads applied were estimated according to the measurements of Jones *et al.* (2012*a*). However, due to lack of extant representatives to test whether the model presented different stress–strain distribution patterns depending on the loads applied, diverse loads (differing by two and three orders of magnitude) were also applied to the model.

Two analyses were performed, one with the loads applied only to the contact surfaces between the opposing elements (Fig. 3E, G) and a second analysis with all the functional surface loaded, simulating the presence of food materials between the right and left elements and, therefore, an even distribution of the loads across the oral surface (Fig. 3F, H). Accordingly, in the left element model, a total of 50 nodes were loaded to simulate the element–element contact, applying 0.02 N per node. To simulate

FIG. 3. Model and finite element (FE) analysis of *Gnathodus bilineatus* P_1 element platforms derived from a dissected articulated skeleton. A, stage where the cycle is best constrained. B, location of 2D FE analysis focused on the ventral domain of the platform. C, dextral and sinistral element transversal section derived from the synchrotron data. D, 2D FE models with the load conditions focused: (1) at the points of element–element contact (black arrows); or (2) distributed across the oral surface simulating the presence of food particles (red and black arrows). The model was anchored at the basal cavity area, in the contact with basal body. E–H, FE analysis results showing: E–F, compressive stress and vectors (arrows); G, H, tensile stress and vectors (arrows); E, G, simulation of element–element loading; F, H, simulation of element–food loading.

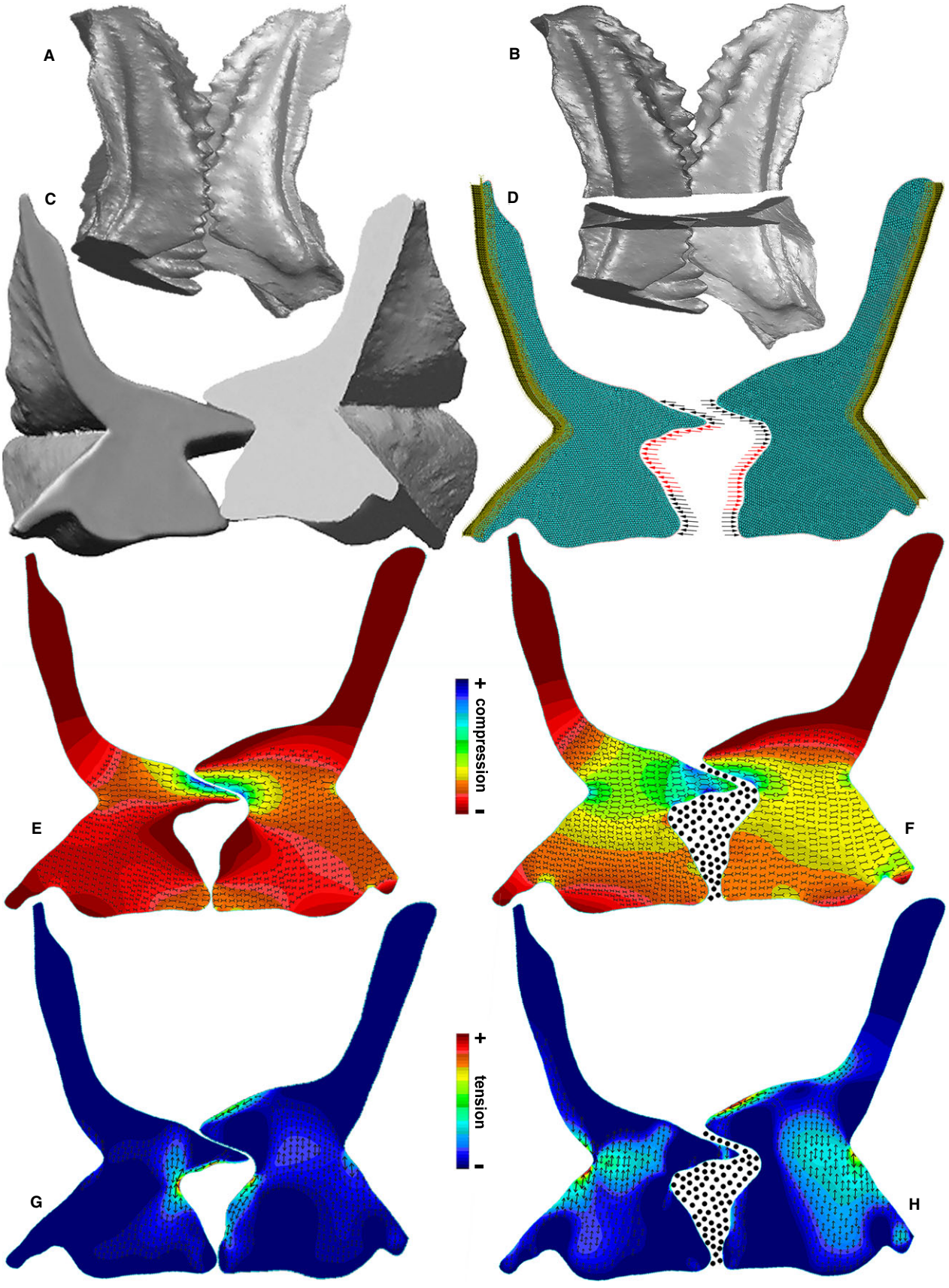
A
B
C
D
E
F
G
H
+ compression -
+ tension -

the element–food model, a total of 112 nodes were loaded with 0.009 N each. The right element model was loaded with 0.02 N per node (49 nodes in total) to simulate the element–element contact model, while for the element–food model 0.01 N per node was applied to 81 nodes. Because we used a linear elastic model to represent the mechanical behaviour of a slice of conodont enamel microstructure, the magnitude of the stress does not affect the pattern of stress distribution, as such we do not infer stress or strain magnitudes, only stress orientations and patterns imposed by simple occlusal loads.

RESULTS

Element occlusion

The P_1 elements of *G. bilineatus* exhibit a ventral free blade and a rostrally and caudally expanded dorsal platform (Fig. 1). The blade extends into a carina that reaches the end of the platform, separated by an intervening trough from a caudal platform of approximately the same height, which is ornamented by ridges oriented perpendicularly to the blade. A shallower parapet extends from the rostral face of the carina and exhibits nodular surface ornamentation (Figs 1 and 2A–B).

Interactions between the P_1 elements were inferred from both physical and digital modelling. Based on their occluded juxtaposition in natural assemblages (Purnell and Donoghue 1997), the oral faces of the element pair were brought together bilaterally, with the blade of the sinistral element behind the dextral element, acting as guides and aligning the elements for the approach of the platforms during the occlusal cycle. In this position, the oral faces of the platforms interlock, with a principal point of rotational articulation in the ventral part of the caudal platform (Fig. 2C, E). The more complex oral morphology in this area, with the medial groove and a complex perpendicular arrangement of furrows and troughs on the caudal platform (Fig. 2A–B), constrains the relative motion of the two platforms, facilitating their precise occlusion. As the process of platform occlusion proceeds about this point of articulation, the mid-dorsal regions of the platforms are brought into contact (Fig. 2D, F). The simpler oral surface ornamentation of this region of the platform suggests that occlusion is less precise. The rostral parapets of the opposing elements do not occlude.

Microwear

Microwear textures were identified on the oral surface of the platform and the tips of the denticles in the adjacent blade. As in previous studies, surface damage is most evident along the crest of the blade in the ventral part of the platform (Donoghue and Purnell 1999*b*; Purnell and Jones 2012), with worn cusps and smooth polishing of original surface microtexture on the occlusal side of the blade and on the crests of the adjacent ridges of the ventral platform (Fig. 2G), consistent with contact between elements. At their tips, both sides of denticles exhibit polishing (Fig. 2H), suggesting either contact between elements without food or with nonabrasive food (Purnell 1995). Denticle tips also exhibit spalling (Purnell and Jones 2012); in a few cases, this occurs on the nonocclusal side of the blade (Fig. 2H). No evidence of wear was found on the dorsal part of the platform or on the rostral parapet.

Microstructure

The crown tissue of the elements is organized into three principal microstructural domains:

1. The *free blade*, composed of layers of hydroxyapatite crystallites arranged subparallel to external oral surfaces (Fig. 2J).
2. The *ventral domain*, where the blade joins the platform, characterized in transverse section by crystallites organized in an asymmetrical 'V'-shape whose apex occurs at the tip of the basal cavity. The crystallites in the outer layer arranged perpendicular to the surface (Fig. 2K–L) and lateral areas of this domain characterized by interwoven prisms arranged in outwardly diverging cones, fanning orthogonal to the external surface (Fig. 2I, K–L).
3. The *dorsal domain*, exhibiting comparatively simple microstructural organization, with crystallites oriented perpendicular to the outer surface in parallel layers (Fig. 2I).

Finally, the rostral parapet is composed of layers of hydroxyapatite crystallites arranged subperpendicular to the oral surface (Fig. 2K–L).

FE analysis

Load conditions were informed by analysis of occlusion and wear, assuming that the load was (1) focused at the points of element–element contact or (2) distributed across the oral surface by intervening food items. 2D FE analysis was focused on the ventral domain, the region for which occlusion is best constrained (Fig. 3A–C). In both simulations, compressive stresses are concentrated at the points of element–element contact, most especially on the rostral most occlusal surface, directly overlying the apex of the basal cavity (Fig. 3E–F). However, the element–food model shows a broader distribution of com-

pressive stress through the platform, with a stress peak at the apex of the basal cavity of the right and left elements (Fig. 3F). In both models, the compressive stress trajectories are oriented approximately perpendicular to the oral surface (Fig. 3E–F). In the element–element model, tensile stresses are focused close to the oral surface in nonocclusal areas, but also above and marginal to the apex of the basal cavity (Fig. 3G); in the element–food model, tensile stresses are principally concentrated deep beneath the oral surface, above and marginal to the apex of the basal cavity (Fig. 3H). In both models, tensile stresses are oriented approximately parallel to the oral surface (Fig. 3G–H). Finally, in all the elements and simulations, the nonocclusal rostral parapet shows the lowest compressive and tensile stresses.

DISCUSSION

Our occlusal analysis demonstrates that the opposed, molar-like P_1 elements of *G. bilineatus* exhibit interpenetrative occlusion. The principal point of articulation occurs at the ventral end of the caudal platform (Fig. 2C). Here, the complex morphology of medial groove combined with furrows and troughs constrains the relative motion of elements and facilitates precise occlusion. Occlusion is less precise in the mid-dorsal region of the platforms where the oral morphology is simpler (Fig. 2A–B). These results suggest a model in which the elements occluded in a short rotational movement from ventral to dorsal following the curvature of the oral surface of the element. This hypothesis is supported by our evidence of surface damage, which is concentrated in the ventral region of the platform, particularly along the crest of the blade and on the adjacent ridges of the caudal platform (Fig. 2G). The presence of spalls on both the occlusal and nonocclusal sides of the blade indicates that malocclusion occurred in life, and this could only have happened if the opposing denticle tips were separated, presumably to facilitate either the insertion of food during the occlusal cycle or occlusion of the dorsal parts of the platform. However, the low frequency of spalls, compared with other species (Jones *et al.* 2012*a*), suggests that the complex platform morphology constrained the articulation of the opposing elements, minimizing malocclusion.

The occlusal cycle of *G. bilineatus* is closely comparable with that described for *Wurmiella,* which also shows evidence for episodic separation of the opposing elements, although the simple blade-like elements of *Wurmiella* lacked intrinsic occlusal constraints (Jones *et al.* 2012*a*). *Idiognathodus* also had rotational occlusion (Donoghue and Purnell 1999*a*), and the similarities in the kinematic models for occlusion in these three taxa suggest that this may be a general functional model for P_1 elements that have, or are derived from, blade-like morphologies.

The 2D FE analysis of the ventral domain revealed that topological variations in the pattern of compressive and tensile stress distribution coincide with variations in the element microstructure, particularly in our more realistic model that, to account for the presence of food, distributes the occlusal load across the oral surface. Highest compressive stress occurs at the central part of the platform where the crystallites are optimally aligned to resist compression, with their axes parallel to the compressive stress trajectories (Fig. 3E–F). Conversely, the areas of highest tensile stress (the principal factor in the fracture of brittle materials; Rensberger 1995) are found around the basal cavity and in the middle region of the platform, characterized by a complex arrangement of interwoven prisms, the intersecting boundaries between which are approximately aligned with the main tensile stress trajectories (Fig. 3G–H). These heterogeneities in tissue microstructure would have served as decussation planes, decussating cracks forming in response to tensile stresses and preventing complete failure of the brittle enamel-like tissue in these regions, just as in the enamel microstructure of other vertebrate teeth (Rensberger 1995). Finally, in the most dorsal part of the platform, where we predict that the elements did not occlude and there is no evidence of wear, the microstructure is effectively homogeneous. Therefore, co-variation between predicted stress and microstructural complexity provides powerful corroborative support to the hypothesis that the microstructural complexity of conodont crown tissue is an adaptation to the tooth functions performed by conodont elements.

CONCLUSIONS

Our analyses provide several complementary lines of evidence, supporting the hypothesis that the P_1 elements of *G. bilineatus* functioned efficiently as teeth. Elements rotated in the transverse plane of the anterior–posterior axis through an occlusal cycle that involved separation to facilitate the insertion of food materials. Commonalities in the occlusion kinematics of other conodont taxa suggest that this may be a general functional model for occlusal elements. FE analysis informed by the occlusal and microwear data reveals co-variation of microstructure with compressive and, in particular, tensile stresses. This supports the hypothesis that the microstructural complexity of conodont elements is a functional adaptation (Donoghue 2001). Our integrative study provides a model for functional analysis in other conodont taxa and a functional milieu for interpretation of conodont taxonomy, which is based largely on P_1 element morphology.

Acknowledgements. The work was partially funded by Marie Curie FP7-People IEF 2011-299681 and postdoctoral fellowship from the Fundación Española para la Ciencia y la Tecnología (to CMP). The authors thank Dr. Federica Marone and Dr. Marco Stampanoni (Paul Scherrer Institute) for help at the beamline.

Editor. Zerina Johanson

REFERENCES

BLIECK, A., TURNER, S., BURROW, C. J., SCHULTZE, H. P., REXROAD, C. B., BULTYNCK, P. and NOWLAN, G. S. 2010. Fossils, histology, and phylogeny: why conodonts are not vertebrates. *Episodes*, **33**, 234–241.

DONOGHUE, P. C. J. 1998. Growth and patterning in the conodont skeleton. *Philosophical Transactions of the Royal Society of London, Series B*, **353**, 633–666.

—— 2001. Microstructural variation in conodont enamel is a functional adaptation. *Proceedings of the Royal Society of London, Series B: Biological Sciences*, **268**, 1691–1698.

—— and ALDRIDGE, R. J. 2001. Origin of a mineralised skeleton. 85–105. *In* AHLBERG, P. E. (ed.). *Major events in early vertebrate evolution: palaeontology, phylogeny, genetics and development*. Taylor & Francis, London, 418 pp.

—— and PURNELL, M. A. 1999*a*. Mammal-like occlusion in conodonts. *Paleobiology*, **25**, 58–74.

—— —— 1999*b*. Growth, function, and the fossil record of conodonts. *Geology*, **27**, 251–254.

—— BENGTSON, S., DONG, X.-P., GOSTLING, N. J., HULDTGREN, T., CUNNINGHAM, J. A., YIN, C., YUE, Z., PENG, F. and STAMPANONI, M. 2006. Synchrotron X-ray tomographic microscopy of fossil embryos. *Nature*, **442**, 680–683.

HASS, W. H. 1941. Morphology of conodonts. *Journal of Paleontology*, **15**, 71–81.

JONES, D., EVANS, A. R., SIU, K. K. W., RAYFIELD, E. J. and DONOGHUE, P. C. J. 2012*a*. The sharpest tools in the box? Quantitative analysis of conodont element functional morphology. *Proceedings of the Royal Society of London, Series B: Biological Sciences*, **279**, 2849–2854.

—— —— RAYFIELD, E. J., SIU, K. K. W. and DONOGHUE, P. 2012*b*. Testing micro structural adaptation in the earliest dental tools. *Biology Letters*, **8**, 952–955.

MURDOCK, D. J. E., DONG, X.-P., REPETSKI, J. E., MARONE, F., STAMPANONI, M. and DONOGHUE, P. C. J. 2013. The origin of conodonts and of vertebrate mineralized skeletons. *Nature*, **502**, 546–549.

PURNELL, M. A. 1994. Skeletal ontogeny and feeding mechanisms in conodonts. *Lethaia*, **27**, 129–138.

—— 1995. Microwear in conodont elements and macrophagy in the first vertebrates. *Nature*, **374**, 798–800.

—— and DONOGHUE, P. C. J. 1997. Architecture and functional morphology of the skeletal apparatus of ozarkodinid conodonts. *Philosophical Transactions of the Royal Society of London, Series B: Biological Sciences*, **352**, 1545–1564.

—— and JONES, D. O. 2012. Quantitative analysis of conodont tooth wear and damage as a test of ecological and functional hypotheses. *Paleobiology*, **38**, 605–626.

RENSBERGER, J. M. 1995. Determination of stresses in mammalian dental enamel and their relevance to the interpretation of feeding behaviors in extinct taxa. 151–172. *In* THOMASON, J. (ed.). *Functional morphology in vertebrate paleontology*. Cambridge University Press, Cambridge, 296 pp.

SANSOM, I. J., SMITH, M. P. and SMITH, M. M. 1994. Dentine in conodonts. *Nature*, **368**, 591.

TURNER, S., BURROW, C. J., SCHULTZE, H. P., BLIECK, A., REIF, W.-E., REXROAD, C. B., BULTYNCK, P. and NOWLAN, G. S. 2010. False teeth: conodont-vertebrate phylogenetic relationships revisited. *Geodiversitas*, **32**, 545–594.